Equilibrium phases of tilted dipolar lattice bosons

PAPER • OPEN ACCESS

Equilibrium phases of tilted dipolar lattice bosons

New Journal of Physics
The open access journal at the forefront of physics

Deutsche Physikalische Gesellschaft DPG
IOP Institute of Physics

Published in partnership with: Deutsche Physikalische Gesellschaft and the Institute of Physics

OPEN ACCESS

RECEIVED
2 September 2015

REVISED
16 November 2015

ACCEPTED FOR PUBLICATION
18 November 2015

PUBLISHED
10 December 2015

PAPER

Equilibrium phases of tilted dipolar lattice bosons

C Zhang[1], **A Safavi-Naini**[2], **Ana Maria Rey**[2] **and B Capogrosso-Sansone**[1,3]

[1] Homer L. Dodge Department of Physics and Astronomy, The University of Oklahoma, Norman, OK 73019, USA
[2] JILA, National Institute of Standards and Technologoy and Department of Physics, University of Colorado, 440 UCB, Boulder, CO 80309, USA
[3] Department of Physics, Clark University, Worcester, MA 01610, USA

E-mail: chao.zhang@ou.edu

Keywords: quantum phase transition, quantum gases, quantum phases

Abstract

The recent advances in creating nearly degenerate quantum dipolar gases in optical lattices are opening the doors for the exploration of equilibrium physics of quantum systems with anisotropic and long-range dipolar interactions. In this paper we study the zero- and finite-temperature phase diagrams of a system of hard-core dipolar bosons at half-filling, trapped in a two-dimensional square optical lattice. The dipoles are aligned parallel to one another and tilted out of the optical lattice plane by means of an external electric field. At zero-temperature, the system is a superfluid (SF) at all tilt angles θ provided that the strength of dipolar interaction is below a critical value $V_c(\theta)$. Upon increasing the interaction strength while keeping θ fixed, the SF phase is destabilized in favor of a checkerboard or a stripe solid (SS) depending on the tilt angle. We explore the nature of the phase transition between the two solid phases, identifying a region of metastable emulsion states intervening between the two solid lobes. Additionally, we study the stability of these quantum phases against thermal fluctuations and find that the SS is the most robust, making it the best candidate for experimental observation.

1. Introduction

Experimental progress in trapping and controlling ultra cold atoms and molecules has led to the observation of magnetic and electric dipolar interactions in a variety of systems [1–13]. These systems can be used as quantum simulators to study quantum transport and dynamical and equilibrium properties of models featuring long-range and anisotropic dipolar interactions. Long-range dipolar interactions have been predicted to stabilize a plethora of exotic quantum phases such as p-wave superfluids (SFs), SFs of multimers, charge density waves, stripe solids (SSs), and supersolids. Moreover, dipolar interactions play an important role in many models of strongly correlated systems, excitons with spatially separated electrons and holes [14–16], and frustrated quantum magnets [17–19].

The recent success in creating a gas of polar molecules in an optical lattice is the first step towards the realization of a low-entropy initial state which is a key ingredient for creating a quantum simulator [7, 20, 21] built using electric dipoles. Similarly the recent progress in loading Er atoms in an optical lattice, accompanied by the observation of modifications of the SF to MI transition [22] is a groundbreaking step toward simulating quantum magnetism using magnetic dipoles. The ability to change the alignment of the dipole moment by applying an external field has sparked numerous studies on the many-body phases of dipolar gases. Many-body bosonic and fermionic dipoles with dipoles aligned perpendicular to the lattice or parallel to the lattice have been studied extensively [23–31]. However, the theoretical and numerical effort to study dipolar gases with dipoles aligned at arbitrary tilt angles has either focused on continuous systems [32–41] or has employed non-exact methods such as functional renormalization group [42], mean field theory and variational approaches [43–45]. In particular, soft-core dipolar bosons trapped in optical lattices have been found to stabilize a variety of phases which include SF, checkerboard solid (CB), supersolid, SS, depending on the geometry of the system and the filling factor.

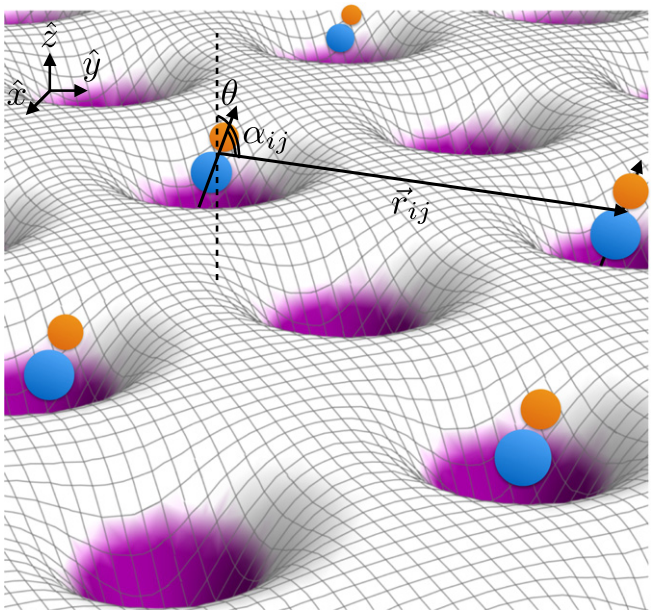

Figure 1. Schematic representation of the system. Dipoles are trapped in a two-dimensional optical lattice and are aligned parallel to each other along the direction of polarization, determined by an electromagnetic field. We assume that the external electric field points along the z–y plane, with polar angle θ and azimutal angle $\phi = \pi/2$. The anisotropic dipolar interaction depends on the angle α_{ij} between the direction of polarization and the relative position of particles.

In the following we present a systematic study of a system of hard-core, dipolar bosons trapped in a two-dimensional square lattice. We treat the alignment of the dipoles as a parameter which can be adjusted via the application of an external field. We use the worm algorithm (WA) [46], a type of path integral quantum Monte Carl (QMC) method, and study the zero- and finite-temperature phase diagrams of the system at *half-filling* as a function of the tilt angle and the strength of dipolar interaction. We find that at low interaction strength the system is in the SF state for any value of the tilt angle. Upon increasing the interaction strength the SF phase is destabilized in favor of either a CB or a SS depending on the tilt angle. In the transition region between the two solid phases we observe metastable phases consisting of coexisting domains of the two solids. Additionally, we study the robustness of these quantum phases against thermal fluctuations and show that the solid phases survive at temperatures higher than the critical temperature for the disappearance of the SF phase. In particular, due to the anisotropy of the dipolar interaction, the SS turns out to be the most robust phase, making it the best candidate for experimental observation. We give predictions for actual experimental setups and temperatures required to observe solid phases.

This paper is structured as follows: in section 2 we discuss the Hamiltonian describing the system. In section 3 we present the zero and finite-temperature phase diagrams. In section 4 we discuss how harmonic confinement affects our results. In section 5 we explore possible experimental realizations and provide temperature estimates. Finally, section 6 concludes the paper.

2. Hamiltonian

We study a system of hardcore, dipolar bosons with induced dipole moment d, confined by a two-dimensional square optical lattice with lattice constant a and by an external harmonic trap. A schematic representation of this setup, in the absence of the external confinement, is shown in figure 1. Dipoles are aligned parallel to each other along the direction of polarization, determined by an electromagnetic field which we assume points along the z–y plane, with polar angle θ and azimutal angle $\phi = \pi/2$. The system is described by the Hamiltonian

$$H = -J\sum_{\langle i\,j\rangle} a_i^\dagger a_j + V\sum_{i<j}\frac{n_i n_j}{r_{ij}^3}\left(1 - 3\cos^2\alpha_{ij}\right) - \sum_i \mu_i n_i, \tag{1}$$

where the first term describes the kinetic energy of the system with hopping energy J and the second term is the dipole-dipole interaction with strength $V \propto d^2/a^3$ and $r_{ij} = |\vec{r_i} - \vec{r_j}|$. α_{ij} characterizes the angle between the direction of the polarization and the relative position of the two particles given by $\vec{r}_{ij}$. Here, $a_i^\dagger$ (a_i) are the bosonic creation (annihilation) operators with the usual commutation relations and $n_i = a_i^\dagger a_i$.The hard-core condition $a_i^{\dagger 2} = 0$ implies that sites with more than one atom are energetically suppressed due to a large onsite interaction

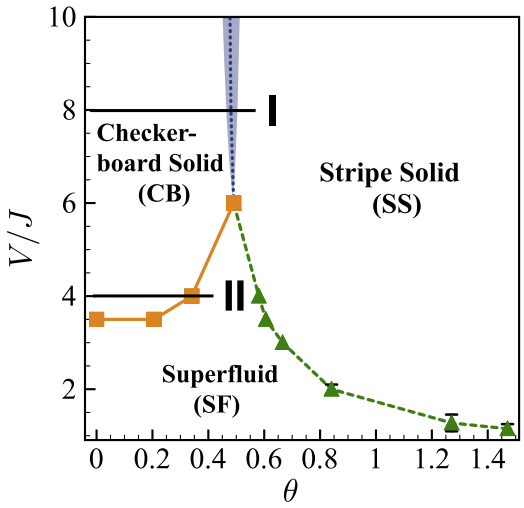

Figure 2. Zero-temperature phase diagram of the system described by equation (1) as a function of tilt angle θ and V/J, and in the absence of harmonic confinement. The system features a checkerboard solid (CB), a stripe solid (SS), and a superfluid phase (SF). The CB-SS transition features a region in parameter space where metastable emulsions intervening between the two phases are present (shaded area). This may be a signature of a first-order phase transition, or an emulsion phase separating the two solids. If error bars are not visible they are within symbol size.

energy penalty. In this limit the usual onsite interaction term of the Bose–Hubbard model does not play any role. We use $\langle ...\rangle$ to denote nearest neighboring sites. Finally, $\mu_i = \mu - \sum_{\xi=x,y} w_\xi \xi_i^2$, where w_ξ and ξ_i are the strength of harmonic confinement and the coordinate of site i along axis ξ, respectively, and μ is the chemical potential which sets the total number of particles.

3. Zero- and finite-temperature phase diagrams

In this section, we present the zero- and finite-temperature phase diagrams of the system described by equation (1) at half-filling and in the absence of an external harmonic confinement. The chemical potential is set to ensure the half filling condition, $n = N/N_{\text{sites}} = 0.5$. The effect of the harmonic confinement is discussed in section 4. Our results are based on path integral QMC simulations using the WA. Unless otherwise noted, we simulate systems with spacial dimensions $L \times L$, where $L = 24, 30, 36$, and 42, with $N_{\text{sites}} = L \times L$ and use periodic boundary conditions. To extract the ground state phase diagram, we work at inverse temperature $\beta = L/J$ which ensures that the system is effectively at zero temperature.

The main panel in figure 2 shows the zero-temperature phase diagram in the $V/J - \theta$ plane which features three phases: a SF phase, a CB solid phase, and a SS phase. The SF phase possesses off-diagonal long-range order and is characterized by finite SF stiffness ρ_s, which can be extracted from simulations by measuring the winding number in space $\rho_s = m\langle \mathbf{W}^2\rangle / dL^{d-2}\beta$ [47]. The diagonal order in the solid phases is characterized by a finite value of structure factor $S(\mathbf{k}) = \sum_{\mathbf{r},\mathbf{r}'} \exp[i\mathbf{k}(\mathbf{r} - \mathbf{r}')]\langle n_{\mathbf{r}} n_{\mathbf{r}'}\rangle / N$, where $\mathbf{k}$ is the reciprocal lattice vector. We use $\mathbf{k} = (\pi, \pi)$ and $\mathbf{k} = (0, \pi)$ to identify the CB and SS phases, respectively.

At low interaction strength, the system is in a SF phase for any value of the tilt angle θ. The SF phase is destabilized towards a solid phase as the interaction is increased above a critical value $V_c(\theta)/J$. Filled squares mark the onset of the CB solid, which forms at lower θ, while filled triangles mark the onset of the stripe phase which appears at larger θ.

Using energy considerations, it is easy to see that the anisotropic nature of the dipolar interaction leads to the stabilization of the CB solid at $\theta = 0$ and the SS phase at $\theta = \pi/2$. Moreover we observe that at larger values of the tilt angle the SF phase is less stable against increasing the dipolar interaction strength. Indeed, at a tilt angle $\theta = \pi/2$, the dipolar interaction strength needed to destroy superfluidity in favor of a solid is about a factor of two smaller than what needed at a tilt angle $\theta = 0$. At intermediate tilt angles, $\theta \sim \pi/6$, the competition between the two solid orders renders both unstable. This adds to the robustness of the SF phase, where a dipolar interaction $V/J \sim 6$ is required in order to destroy the off-diagonal long range order.

We find the solid-SF transition points by studying finite size effects on ρ_s and $S(\mathbf{k})$. We determine the error bars for the solid to SF transition by monitoring the order parameters characterizing the two phases, namely ρ_s and $S(\mathbf{k})$. We assure that the order parameter characterizing the solid phase vanishes with increasing system size as we cross the phase boundary to the SF phase and vice versa.

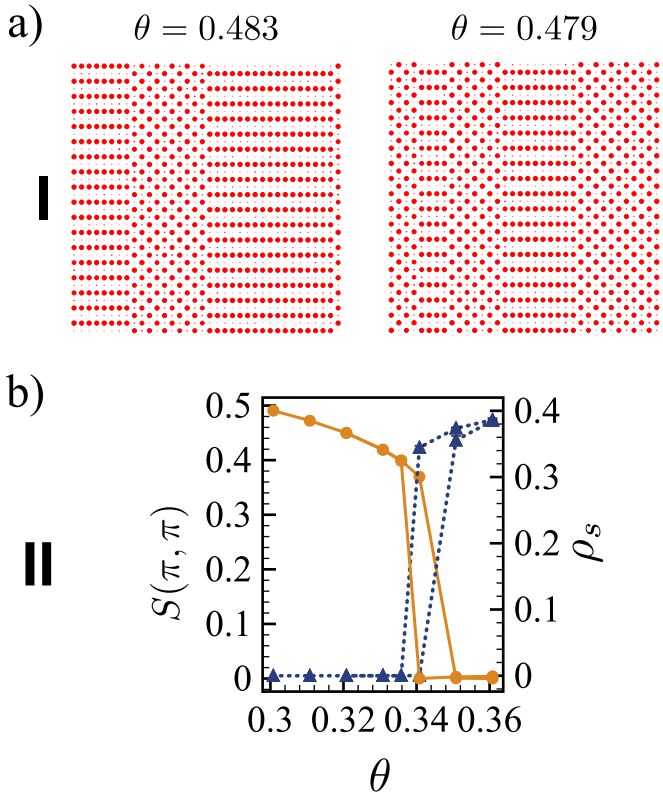

Figure 3. The behavior of the system along cuts I and II. (a) The density distribution of the system along cut I through the shaded region in figure 2 at two values of θ shows evidence of micro emulsion phase. Here, each circle corresponds to a different site, and its radius is proportional to the local average density. (b) The CB structure factor $S(\pi, \pi)$ and superfluid density ρ_s as a function of θ along cut II. We find evidence of hysteresis which indicates that this transition behaves as a weak first-order phase transition for finite systems.

Given the nature of the interaction and the dimensionality of the system, as a function of density, a phase transition between two ordered states is not allowed [25, 48–50]. Instead, a micro-emulsion phase where a mesoscale mixture of phases is present intervenes between the two ordered states. However, in the following we study the phase transitions at fixed density, while varying the interaction strength. First we investigate the phase transition between the CB and SS phases at $V/J = 8$. To this end we perform scans along the cut marked I on the main panel of figure 2. We provide examples of the density map of the system in this region in figure 3(a). Here, each small dot shows an empty lattice site, while the larger circles indicate sites with unit or nearly unit filling. In this region, the system features various metastable emulsion phases of the SS and CB solid. The density maps shown in figure 3(a) show regions of SS and CB phase separated by domain walls. This metastability persists for system sizes up to $L = 100$ studied in this work, with the shape of the emulsion domains varying depending on the initial conditions of the simulation. The presence of metastability indicates that the transition is not a second-order phase transition. However, metastability can be attributed to two different scenarios: first-order transition between the two solids, or an emulsion region separating the two phases. At present we are not able to distinguish between the two.

We have also investigated the nature of the CB-SF phase transition by performing a similar scan along $V/J = 4$ line labeled as II, for a system with $L = 100$. In figure 3(b) we plot the structure factor $S(\pi, \pi)$ as a function of θ using filled circles. The SF density ρ_s is shown using filled triangles. We observe hysteresis in both $S(\pi, \pi)$ and ρ_s with a width of the hysteresis loop of only $\Delta\theta \sim 0.015$. This observation suggests that the system undergoes a weak first-order phase transition. It should be noted that we have not observed an emulsion phase intervening between the SF and the CB phase for system sizes up to $L = 100$. Hence if the emulsion phase exists, the size of emulsion would be larger than this lattice size, and correspondingly large systems should be used in order to observe it experimentally. It should be noted that we have not found a region in the parameter space where diagonal and off-diagonal order coexist. This indicates that there is no supersolid phase intervening between the SF and either of the solid phases.

Next we present an investigation of the robustness of the quantum phases described above against thermal fluctuations. As expected, we find the solid phases to be the most robust against thermal fluctuations. We have performed scans over V/J at two tilt angles $\theta = 0.271$ and $\theta = 0.84$ corresponding to SF-CB and SF-SS

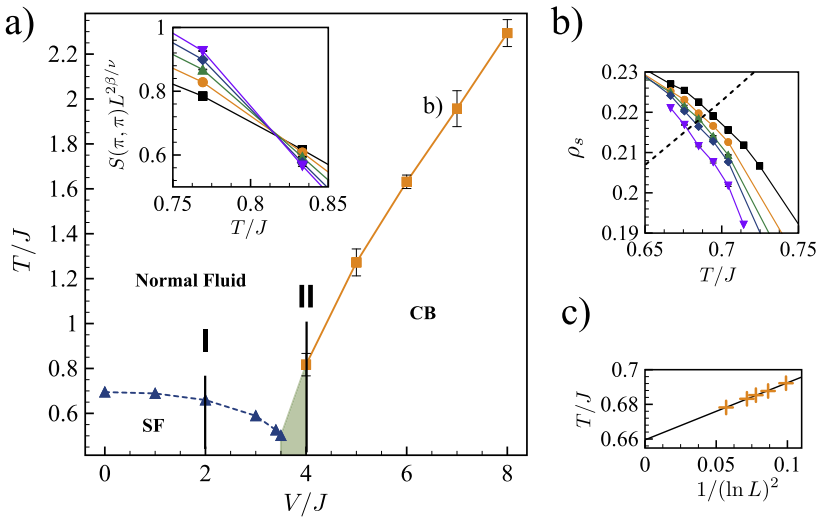

Figure 4. (a) Finite temperature phase diagram at tilt angle $\theta = 0.271$. Upon increasing the temperature, thermal fluctuations destroy the CB and SF order in favor of a normal fluid. The CB phase melts via a two-dimensional Ising transition. The inset shows the scaled structure factor with $2\beta/\nu = 0.25$ for $L = 18, 24, 36, 42, 48$ along cut II, at $V/J = 4$. The crossing determines the critical temperature $T_c/J = 0.812 \pm 0.002$. The SF-normal fluid transition is a Kosterlitz–Thouless phase transition. In (b) we show ρ_s as a function of T/J for $L = 24, 36, 42, 48$, and 66 along cut I at $V/J = 2$. The dashed line is given by T/π. In (c) we use the intersection points between the T/π line and the ρ_s versus T/J curves at each L to extract $T_c/J \approx 0.66$.

transitions at zero temperature. Our results for $\theta = 0.271$ are summarized in figure 4. The phase boundaries are extracted from finite size scaling analysis of ρ_s and $S(\pi, \pi)$. We were not able to resolve the phase boundaries within the shaded region with the system sizes considered in this paper. Within this region we expect the system to undergo either a weak first order phase transition or feature a micro-emulsion phase at zero temperature. Upon increasing the temperature, thermal fluctuations destroy the SF phase in favor of a normal fluid via a Kosterlitz–Thouless (KT) transition [51]. In figure 4(b) we show ρ_s as a function of T/J for $L = 24, 36, 42, 48$, and 66 at $V/J = 2$, indicated as cut I in figure 4(a). In the thermodynamic limit, a universal jump is observed at the critical temperature given by $\rho_s(T_c) = 2mk_B T_c/\pi\hbar^2$. In a finite size system this jump is smeared out as seen in figure 4(b). To extract the critical temperature in the thermodynamic limit, we apply finite-size scaling to $T_c(L)$. From renormalization-group analysis one finds $T_c(L) = T_c(\infty) + \dfrac{c}{\ln^2(L)}$, where c is a constant and $T_c(L)$ is determined from $\rho_s(T_c, L) = 2mk_B T_c/\pi\hbar^2$ [52–54]. We therefore extract the critical temperature as shown in figures 4(b) and (c). The dashed line in figure 4(b) corresponds to $\rho_s = T/\pi$ and its intersection points with each ρ_s versus T/J curve are used to find T_c as shown in figure 4(c). We find $T_c/J \approx 0.66$ at $V/J = 2$. The CB solid melts in favor of a normal fluid via a two-dimensional Ising transition. We use standard finite size scaling as shown in the inset of figure 4 where we plot the scaled structure factor $S(\pi, \pi)L^{2\beta/\nu}$, with $2\beta/\nu = 0.25$ as a function of T/J for $L = 18, 24, 36, 42, 48$ along cut II, at $V/J = 4$. The crossing indicates a critical temperature $T_c/J = 0.812 \pm 0.002$.

We have performed a similar analysis at fixed tilt angle $\theta = 0.84$ where the zero-temperature phase diagram features the SF and SS phases. The results are shown in figure 5(a). Critical temperatures are found using the same methods as described for the SF and CB phases. It is worth noting that while both the SS and CB phases are more robust against thermal fluctuations compared to the SF phase, at any given V/J the SS phase has critical temperature roughly twice that of the CB phase.

Finally, we look at the finite temperature properties of the metastable CB-SS region at $V/J = 8$. In figure 5(b) we show $S(\mathbf{k})$ for the CB and SS phases as a function of T/J at $\theta \approx 0.48$ and $L = 100$. We use squares and circles to show $S(\pi, \pi)$ and $S(\pi, 0)$, respectively. The filled and open symbols correspond to two different initial conditions chosen for the simulations at each T/J. Since the equilibrium density distribution of these metastable phases is affected by the choice of initial conditions, we observe large fluctuations in $S(\mathbf{k})$. We find that at $T/J \gtrsim 1.2$ the system is in the normal fluid phase, with both SS and CB phases disappearing. If $T/J < 1.2$ the metastable phase can be dominated by either solid order, depending on the initial conditions.

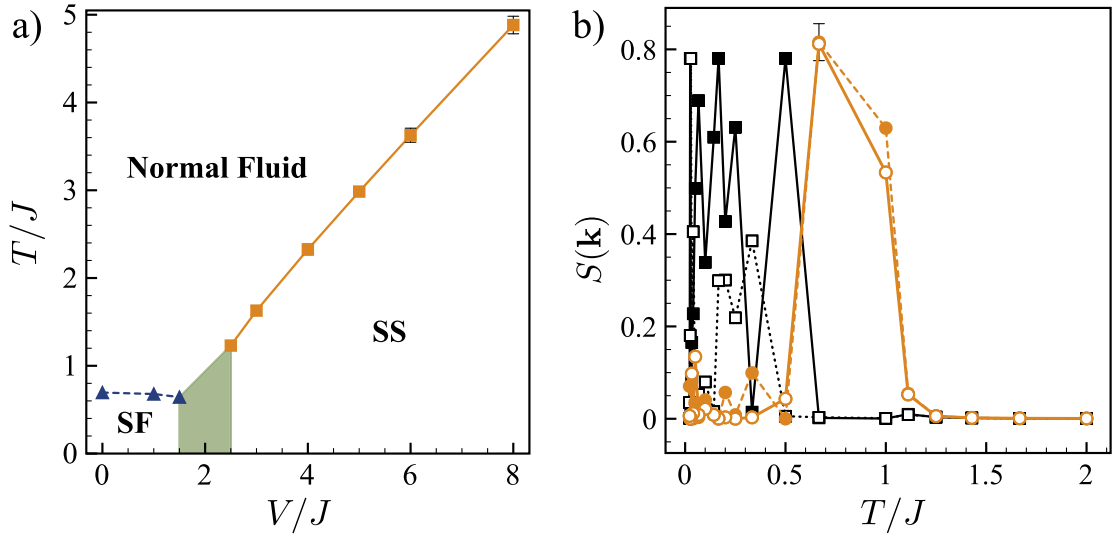

Figure 5. (a) Finite temperature phase diagram at tilt angle $\theta = 0.84$. Critical temperatures are found using the same methods as described for the data in figure 4. (b) Finite temperature properties of the CB-SS metastable phases at $V/J = 8$, $\theta \approx 0.48$, and $L = 100$. Squares and circles correspond to $S(\pi, \pi)$ and $S(\pi, 0)$, respectively. Filled and empty symbols refer to different initial conditions. At $T/J \gtrsim 1.2$ the system is in the normal fluid phase, while at $T/J < 1.2$, the metastable phase is dominated by either solid order, depending on the initial conditions.

4. Harmonic confinement

In a typical experimental system particles are subject to the optical lattice potential as well as an external harmonic confinement. The effect of the harmonic confinement can be taken into account in the QMC simulations through a site-dependent chemical potential as shown in Hamiltonian (1).

The variation of the chemical potential provides a scan over density hence resulting in coexistence of phases realized at half-filling (as described above) with phases stabilized at other fillings. Here we use a harmonic confinement $\omega_\xi/J \approx 0.12$. The top and bottom left panels in figure 6 present the equilibrium density distribution of the dipoles, where each circle corresponds to a different site, and its radius is proportional to the local average density, with the largest radius indicating the presence of one particle on that site.

In the presence of the harmonic trapping potential we cannot use the usual winding number relations to measure the SF density in the different regions of the trap. However we can use the off-diagonal correlator $\langle a^\dagger(\vec{r}_i)\, a(\vec{r}_j)\rangle$, to map the SF regions within the trap. In the panels on the right-hand side of figure 6 we assign a certain brightness to each lattice site. The brightness is inversely proportional to the distance over which the correlator $\langle a^\dagger(\vec{r}_i)\, a(\vec{r}_j)\rangle$ with $\vec{r}_i$ or $\vec{r}_j$ fixed at that lattice site decays. For example, if the correlator does not decay, then that lattice site will be white. Conversely, if the correlator decays exponentially over distances of the order of one lattice constant, that lattice site will be dark.

The top left and right panels correspond to $V/J = 2$, tilt angle $\theta = 1.34$ and $N \sim 511$. The particles at the center of the trap form a MI with unit filling while a SS is stabilized in most of the outer shell. The dark regions in the top right panel indicate an absence of off-diagonal long-range order, corresponding to the SS and MI phases. Given the steepness of the harmonic potential, we do not observe a SF shell separating the two insulating phases, however off-diagonal long-range order is present adjacent to the MI shell. This is due to the mismatch between the symmetry of the SS and the trap, which destabilizes the SS and allows for the build up of phase coherence in this region.

The bottom left and right panels of figure 6 corresponds to $V/J = 6$ and tilt angle $\theta = 0.27$ for which the CB phase is stabilized at half filling. The total number of particles in the trap is $N \sim 1217$. We observe the presence of SF phase at the center of the trap, followed by a shell of CB solid which gives way to a SF outer shell once the harmonic potential is strong enough destroy the solid order. The SF regions are characterized by local density different than 1 and 0.5 as the left panel shows, while off-diagonal long-range order is present as seen in the right panel. On the other hand, the left panel clearly shows a CB structure at density 0.5 in the inner shell with corresponding absence of off-diagonal long-range order (dark color in right panel). We note that the solid phases can be detected using Bragg spectroscopy techniques or single-site imaging [55, 56]. The results presented are similar to what reported for dipolar fermions in [42, 57, 58] where coexistence of phases is observed in the presence of a harmonic confinement.

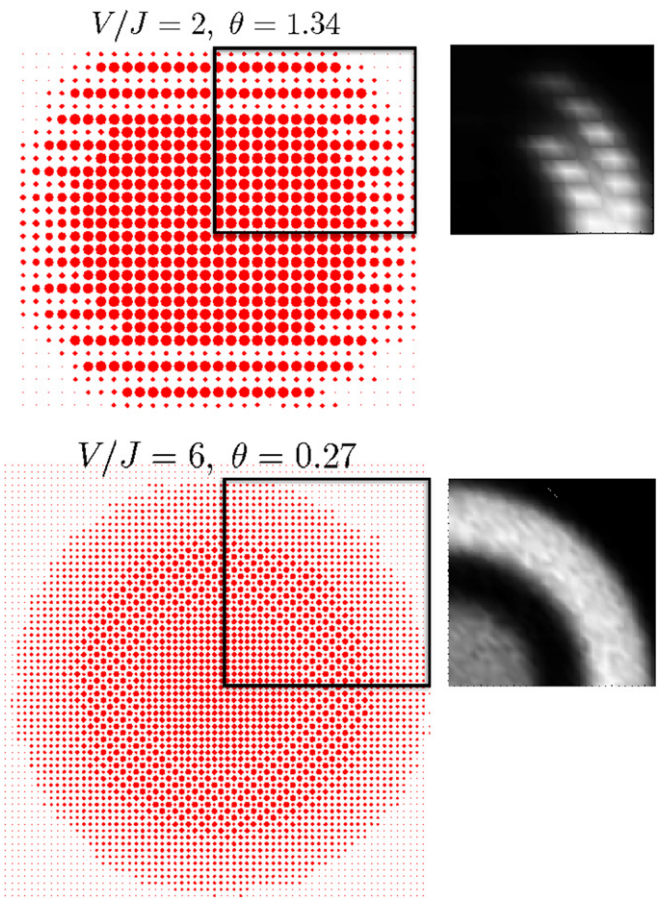

Figure 6. Left panels: density distribution of dipoles in the presence of a harmonic potential (see text). Each circle corresponds to a different site, and its radius is proportional to the local average density. Right panels: statistics of the off-diagonal correlator $\langle a^\dagger(\vec{r}_i)\, a(\vec{r}_j)\rangle$ (see text for detail). A brighter color corresponds to regions of the trap where off-diagonal long-range order is present. Top left and right panels: $V/J = 2$, $\theta = 1.34$, $N \sim 511$. A MI phase with filling factor one is observed at the center of the trap, while a stripe solid is stabilized in most of the outer shell. Bottom left and right panels: $V/J = 6$, $\theta = 0.27$, $N \sim 1217$. A superfluid phase is observed at the center of the trap, followed by a shell of CB solid which gives way to a superfluid outer shell once the harmonic potential is strong enough destroy the solid order.

5. Experimental realization

The system described in section 2 can be experimentally realized using bosonic polar molecules trapped in a two-dimensional square lattice, or systems with magnetic dipolar moments, such as Dy and Er. While the current experiments with magnetic dipoles operate in the soft-core regime [22], the existence of Feshbach resonances allow one to tune the inter-species interactions to approach the hard-core limit [1, 9, 13, 59, 60]. External electric and magnetic fields are used to align electric and magnetic dipole moments, respectively, realizing an interaction term of the form described in equation (1). The equilibrium states in the hard-core regime, such as the ones described above, have not been prepared yet. However, rapid experimental advances will allow for the realization of these states in the future. Our calculations suggest that, unless dipoles are tilted at intermediate angles $\theta \sim \pi/6$, for which superfluidity survives even for suppressed hopping strength $J/V \sim 0.17$, solid phases would be the best candidate for experimental observation since they are more robust against thermal fluctuations. For example, for a system of Er_2 Feshbach molecules [13] with magnetic moment $d = 14\mu_B$, where μ_B is the Bohr magneton, trapped in an optical lattice with lattice constant $a = 532$ nm and depth $V_0 \sim 15E_R$, one gets a hopping rate $J/h \sim 4$ Hz and $V/J \sim 4.3$. Hence, observation of the SS would be possible at temperatures $T \sim 0.5$ nK. For a system of $^{39}K^{87}Rb$ polar molecules with permanent dipole moment $d = 0.57D$, trapped in an optical lattice with lattice constant $a = 532$ nm and depth $V_0 = 10E_R$, one gets a tunneling rate $J/h \sim 30$ Hz and a maximum value (computed at the permanent dipole moment) of $V/J \sim 10$ which results in a temperature $T \sim 10$ nK needed to observe the SS.

Alternatively, a sufficiently deep optical lattice can be used to suppress double occupancy. In this limit, the hard-core condition is valid for all tilt angles. This is particularly relevant to the case of chemically reactive polar molecules, where, for example, a lattice depth of $V_0 = 40E_R$ [7], pins the polar molecules in place. In this system, internal rotational states are used to engineer long-range hopping. In this case, both the hopping and the

interaction terms are determined by the dipole moment of the molecules and the lattice constant, and the corresponding ratio is tunable by electromagnetic fields and choice of rotational levels [7, 19–21]. For instance, for the two lowest rotational states, V/J can be tuned to take values between 0 and 6. The only relevant difference in this implementation compared to the one described above is that the the resulting Hamiltonian features long-range and anisotropic hopping. While this will introduce new features in the phase diagram, for arrays close to unit filling the solid phases will remain robust at similar or larger spin temperatures. It should be noted that in this implementation the two internal states correspond to the full and empty sites.

6. Conclusions

In summary, we presented the zero- and finite-temperature phase diagrams of a system of hard-core, dipolar lattice bosons at half-filling as a function of the alignment of the dipole moments, characterized by the tilt-angle θ, and the strength of the dipolar interaction. At zero-temperature, the system features three phases: SF, CB solid and SS. The SF phase is present at all tilt angles, provided that the interaction strength is below $V_c(\theta)/J$, and upon increasing the interaction strength the system enters one of the two solid phases depending on the value of θ. We observed signatures of a micro-emulsion phase transition, observing an emulsion phase of the CB and SS in the region separating the two solid phases. Finally, we studied the robustness of these phases against thermal fluctuations and showed that the solid phases can be observed experimentally at temperatures up to $\sim$10 nK. A natural extension to the results presented above is the study of the phase diagram presented in figure 2 at different values of the azimuthal angle relative to the lattice basis vector. While we do not expect the appearance of new phases, for angles θ stabilizing the SS in figure 2 and for intermediate values of the azimuthal angle relative to the lattice basis vector we expect the SS to be oriented along the diagonal, i.e. a CB solid, rather than along the axes. A SF region intervening between these two types of SSs is also likely to be present.

Acknowledgments

This work was supported by the NSF (PIF-1415561, PIF-1211914 and PFC- 1125844), AFOSR, AFOSR-MURI, NIST and ARO individual investigator awards. The computation for this project was performed at the OU Supercomputing Center for Education and Research (OSCER) at the University of Oklahoma (OU).

References

[1] Griesmaier A, Werner J, Hensler S, Stuhler J and Pfau T 2005 *Phys. Rev. Lett.* **94** 160401
[2] Lahaye T, Koch T, Fröhlich B, Fattori M, Metz J, Griesmaier A, Giovanazzi S and Pfau T 2007 *Nature* **448** 672–5
[3] Ni K K, Ospelkaus S, de Miranda M H G, Pe'er A, Neyenhuis B, Zirbel J J, Kotochigova S, Julienne P S, Jin D S and Ye J 2008 *Science* **322** 231–5
[4] Ospelkaus S, Pe'er A, Ni K K, Zirbel J J, Neyenhuis B, Kotochigova S, Julienne P S, Ye J and Jin D S 2008 *Nat. Phys.* **4** 622–6
[5] Chotia A, Neyenhuis B, Moses S A, Yan B, Covey J P, Foss-Feig M, Rey A M, Jin D S and Ye J 2012 *Phys. Rev. Lett.* **108** 080405
[6] Wu C H, Park J W, Ahmadi P, Will S and Zwierlein M W 2012 *Phys. Rev. Lett.* **109** 085301
[7] Yan B, Moses S A, Gadway B, Covey J P, Hazzard K R A, Rey A M, Jin D S and Ye J 2013 *Nature* **501** 521–5
[8] Takekoshi T, Reichsöllner L, Schindewolf A, Hutson J M, Le C R, Dulieu O, Ferlaino F, Grimm R and Nägerl H C 2014 *Phys. Rev. Lett.* **113** 205301
[9] Lu M, Burdick N Q and Lev B L 2012 *Phys. Rev. Lett.* **108** 215301
[10] Aikawa K, Frisch A, Mark M, Baier S, Grimm R, Bohn J L, Jin D S, Bruun G M and Ferlaino F 2014 *Phys. Rev. Lett.* **113** 263201
[11] Aikawa K, Frisch A, Mark M, Baier S, Grimm R and Ferlaino F 2014 *Phys. Rev. Lett.* **112** 010404
[12] Park J W, Will S A and Zwierlein M W 2015 *Phys. Rev. Lett.* **114** 205302
[13] Frisch A *et al* 2015 *Phys. Rev. Lett.* **115** 203201
[14] Lerner I V and Lozovik Y E 1981 *Zh. Eksp. Teor. Fiz.* **80** 763
[15] Filinov A, Ludwig P, Lozovik Y E, Bonitz M and Stolz H 2006 *J. Phys.: Conf. Ser.* **35** 197–208
[16] Fedorov A K, Kurbakov I L and Lozovik Y E 2014 *Phys. Rev.* B **90** 165430
[17] Sachdev S 2008 *Nat. Phys.* **4** 173–85
[18] Lacroix C, Mendels P and Mila F 2011 *Introduction to Frustrated Magnetism: Materials, Experiments, Theory* (Heidelberg: Springer)
[19] Wall M L, Hazzard K R A and Rey A M 2014 doi:10.1142/9789814678704_0001
[20] Hazzard K R A *et al* 2014 *Phys. Rev. Lett.* **113** 195302
[21] Gorshkov A V, Manmana S R, Chen G, Demler E, Lukin M D and Rey A M 2011 *Phys. Rev.* A **84** 033619
[22] Baier S, Mark M J, Petter D, Aikawa K, Chomaz L, Cai Z, Baranov M, Zoller P and Ferlaino F 2015 arXiv:1507.03500
[23] Yi S, Li T and Sun C P 2007 *Phys. Rev. Lett.* **98** 260405
[24] Menotti C, Trefzger C and Lewenstein M 2007 *Phys. Rev. Lett.* **98** 235301
[25] Pollet L, Picon J D, Büchler H P and Troyer M 2010 *Phys. Rev. Lett.* **104** 125302
[26] Capogrosso-Sansone B, Trefzger C, Lewenstein M, Zoller P and Pupillo G 2010 *Phys. Rev. Lett.* **104** 125301
[27] Ohgoe T, Suzuki T and Kawashima N 2012 *Phys. Rev.* A **86** 063635
[28] Capogrosso-Sansone B 2011 *Phys. Rev.* A **83** 053611
[29] Capogrosso-Sansone B and Kuklov A B 2011 *J. Low Temp. Phys.* **165** 213–26
[30] Safavi-Naini A, Soyler S G, Pupillo G, Sadeghpour H R and Capogrosso-Sansone B 2013 *New J. Phys.* **15** 013036

[31] Safavi-Naini A, Capogrosso-Sansone B and Kuklov A 2014 *Phys. Rev.* A **90** 043604
[32] Yamaguchi Y, Sogo T, Ito T and Miyakawa T 2010 *Phys. Rev.* A **82** 013643
[33] Sun K, Wu C and Das Sarma S 2010 *Phys. Rev.* B **82** 075105
[34] Parish M M and Marchetti F M 2012 *Phys. Rev. Lett.* **108** 145304
[35] Macia A, Mazzanti F and Boronat J 2012 *Eur. Phys. J.* D **66** 301
[36] Macia A, Hufnagl D, Mazzanti F, Boronat J and Zillich R E 2012 *Phys. Rev. Lett.* **109** 235307
[37] Ruggeri M 2013 arXiv:1305.6007v3
[38] Macia A, Boronat J and Mazzanti F 2014 *Phys. Rev.* A **90** 061601
[39] Sieberer L M and Baranov M A 2011 *Phys. Rev.* A **84** 063633
[40] Block J K, Zinner N T and Bruun G M 2012 *New J. Phys.* **14** 105006
[41] Block J K and Bruun G M 2014 *Phys. Rev.* B **90** 155102
[42] Bhongale S G, Mathey L, Tsai S W, Clark C W and Zhao E 2012 *Phys. Rev. Lett.* **108** 145301
[43] Góral K, Santos L and Lewenstein M 2002 *Phys. Rev. Lett.* **88** 170406
[44] Danshita I and Sá de Melo C A R 2009 *Phys. Rev. Lett.* **103** 225301
[45] Fedorov A K, Kurbakov I L and Lozovik Y E 2013 *J. Phys.: Conf. Ser.* **414** 012036
[46] Prokof'ev N V, Svistunov B V and Tupitsyn I S 1998 *J. Exp. Theor. Phys.* **87** 310–21
[47] Pollock E L and Ceperley D M 1987 *Phys. Rev.* B **36** 8343–52
[48] Ng K O and Vanderbilt D 1995 *Phys. Rev.* B **52** 2177–83
[49] Spivak B 2003 *Phys. Rev.* B **67** 125205
[50] Spivak B and Kivelson S A 2004 *Phys. Rev.* B **70** 155114
[51] Kosterlitz J M and Thouless D J 1973 *J. Phys. C: Solid State Phys.* **6** 1181–203
[52] Kosterlitz J 1974 *Phys.* C **7** 1046
[53] Nelson D R and Kosterlitz J M 1977 *Phys. Rev. Lett.* **39** 1201
[54] Ceperley D and Pollock E 1989 *Phys. Rev.* B **39** 2084–93
[55] Clément D, Fabbri N, Fallani L, Fort C and Inguscio M 2009 *Phys. Rev. Lett.* **102** 155301
[56] Bakr W S, Peng A, Folling S and Greiner M 2009 *Nature* **462** 74
[57] Gadsbølle A L and Bruun G M 2012 *Phys. Rev.* A **85** 021604
[58] Gadsbølle A L and Bruun G M 2012 *Phys. Rev.* A **86** 033623
[59] Maier T, Ferrier-Barbut I, Kadau H, Schmitt M, Wenzel M, Wink C, Pfau T, Jachymski K and Julienne P S 2015 arXiv:1506.01875
[60] Kadau H, Schmitt M, Wenzel M, Wink C, Maier T, Ferrier-Barbut I and Pfau T 2015 arXiv:1508.05007